



Electrical conductivity determination of semiconductors by utilizing photography, finite element simulation and resistance measurement

Rui Wang¹ and Ralf Moos^{1,*}

¹Department of Functional Materials, University of Bayreuth, 95447 Bayreuth, Germany

Received: 2 December 2020

Accepted: 18 February 2021

Published online:
8 March 2021

© The Author(s) 2021

ABSTRACT

A new method is developed to measure precisely and reliably the electrical conductivity of a block-shaped semiconductor specimen using four-wire technique with electrodes in arbitrary shape and position. No effort for accurate electrode preparation is necessary anymore. This method may be especially applied to measure the conductivity of ceramics at high temperatures, when typical spring-contacts or clamp-contacts are not possible and instead wound wires are used for electrically contacting the specimen. The method comprises the following: An image of the specimen is processed to a 3D model. By applying a finite element simulation on this 3D model, a form factor (also called geometry factor) that considers the effect of the non-infinitesimally small electrodes is calculated. Together with the measured resistance (preferably in four-wire technique), the actual conductivity of the sample is derived. Experimental results confirmed the validity of the proposed method. As a limitation of the method, the conductivity of the specimen should be within the range of 0.01 Sm^{-1} and 10^6 Sm^{-1} .

Introduction

Depending on the sample geometry, various methods [1, 2] are developed to measure the conductivity of semiconductors. Basically, the four-point probe technique is often applied to exclude contact resistances. [3, 4]. As for disk-like samples of arbitrary shape, Van der Pauw method [5] is applicable, if the

sample is homogeneous and has no holes. Electrodes have to be infinitesimally small and have to be placed at the edge of the sample. In order to further reduce the measurement error, ASTM F76-08 suggests, for instance, specimens should have the shape of a clover-leaf [6]. One drawback of the Van der Pauw method is that cutting brittle semiconductors, e.g., oxide ceramics, into the required clover-leaf shape is difficult and time-consuming. Especially for ceramics

Handling Editor: David Cann.

Address correspondence to E-mail: functional.materials@uni-bayreuth.de

<https://doi.org/10.1007/s10853-021-05949-4>

to be characterized at high temperatures (i.e., when determining the conductivity vs. oxygen partial pressure, as it is typical for defect chemical considerations [7, 8]), spring-contacts or clamp-contacts are hardly possible. In that case, it is common practice to use block-shaped or plate-like specimens that are sometimes referred to as “bar geometry.” Four wires (for four-wire technique) are wound around the specimens and the wires are connected to the specimens with a noble metal paste. For both the Van der Pauw method and the bar geometry, four-wire technique is appropriate, to exclude contact resistances. A scheme is given in Fig. 1a. Very often the blocks are thin in one dimension to form rectangular-shaped small plates, see, e.g., [9–11]. Under the assumption that the electrodes are parallel and infinitely small, the equipotential surfaces can be considered as flat and equidistant. Thus, the electrical field is homogeneous everywhere in the specimen. The conductivity σ can be directly derived from the current I passing through electrode E_1 and E_4 , and the

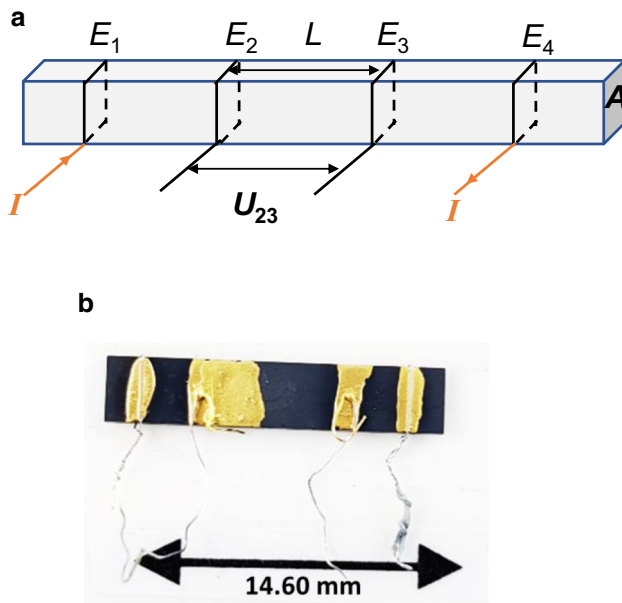


Figure 1 **a** Idealized block-shaped specimen (the specimen has the geometry of a cuboid with the cross-sectional area A). Four electrodes E_1 , E_2 , E_3 and E_4 are contacted to the surface of the sample. These electrodes are infinitely thin and parallel to each other. A current I is introduced into E_1 and E_4 . The potential difference between E_2 and E_3 is measured as U_{23} . **b** A typical specimen with sloppily prepared, wild-looking electrodes as they would be typically not suitable to determine precisely the conductivity due to the undefined L , here even with electrodes only on the top of the specimen).

potential difference U_{23} between electrode E_2 and electrode E_3 , the distance L between electrode E_2 and E_3 , and the area of the cross section A , using

$$\sigma = \frac{I}{U_{23}} \cdot \frac{L}{A} = \frac{I}{U_{23}} \cdot K \quad (1)$$

In this simple geometry, the form factor (or geometry factor) K can be written as $K = L/A$.

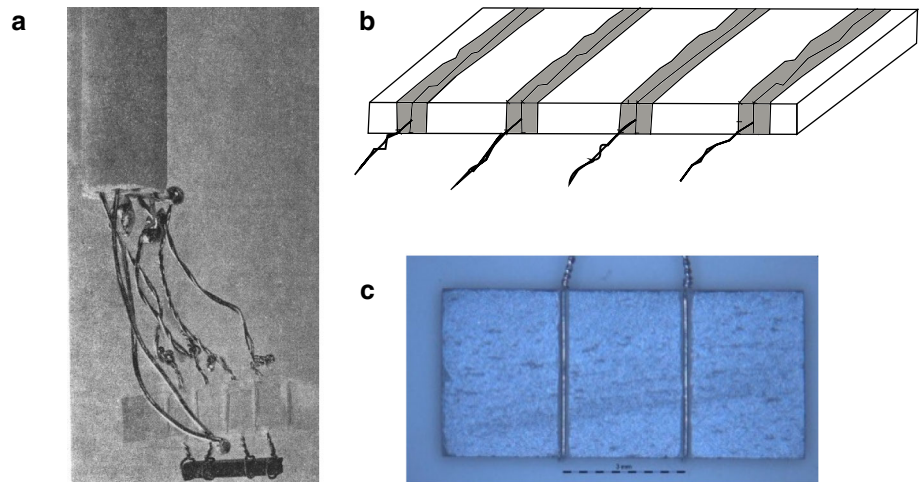
In order to prepare specimens that meet the assumptions above, sometimes even laser engraving is used to make narrow slits where the electrode should be fitted into [11]. Since the specimens usually have dimensions in the mm range, e.g., 10 mm \times 3 mm \times 3 mm [8], or 15 mm \times 5 mm \times 0.3.. 1 mm [10], fitting the thin wires into the slits is conducted under a microscope and their thorough preparation is labor-intensive. Some typical setups from sample as shown in literature are given in Fig. 2. Figure 2c is a typical example for a very precisely prepared specimen, although only in two-wire technique.

In most cases, the slits are not engraved and a conductive paste is used to guarantee a good electrical contact of the electrodes with the specimen. Because the conductive paste is usually applied manually with a small brush, the electrodes are broadened and they have irregular shapes, see, e.g., the deliberately sloppily prepared specimen in Fig. 1b. There, the homogeneous electric field near the electrodes is distorted. Since the electrodes are neither infinitely thin nor parallel to each other, the distance L is no longer trivial to define, and hence, the form factor K cannot be simply set to $K = L/A$ as in Eq. 1. Using FE (finite element) simulation on a simplified example, it is shown that the relative error in the measurement of the conductivity can be at least 20%, if L is taken as the distance between the centerline of the two inner electrodes (see Part I of the Supplementary Information).

Therefore, in order to eliminate the error due to the false determination of L and in order to allow using more or less arbitrarily shaped, especially wide and not well-defined electrode geometries so that the time for precise electrode preparation can be reduced, a new method combining 3D imaging or photography combined with finite element (FE) simulation is developed in this work. It also considers the effect of non-infinitesimally small electrodes.

The basic idea comprises

Figure 2 Typical samples to measure the conductivity of oxide ceramics at high temperatures. **a** from literature for NiO [9], **b** a scheme as used very often with wires and conductor paste, **c** for BICUTIVOX with a very accurately prepared geometry [11].



1. to apply electrodes onto the specimen without any special and/or well-defined geometry,
2. to determine the geometry of specimen and electrodes by appropriate means. This may be any type of 3D scanning or tomography; for flat samples with a known thickness as demonstrated here as a first validation, simple photography can be used to determine the electrode areas,
3. to establish a 3D model of the specimen including the electrodes, with the electrodes being defined as equipotential regions,
4. to calculate a form factor K from the derived 3D model with the help of a Finite element (FE) software tool
5. to measure the resistance or conductance (e.g., by applying I and measuring U), preferably in four-wire technique to avoid contact resistance issues and
6. to calculate the conductivity σ out of the resistance and the derived form factor K .

Theoretical background of the new method

Some assumptions to correctly calculate the form factor apply. First of all, the specimens must be homogeneous and compact. Furthermore, the conductivity of the electrodes must be at least three magnitudes higher than the conductivity of the specimen. This is a precondition, so that the electrode area can be considered as an equipotential area. For the simulation, let us assume the distance of the two inner electrodes if they were infinitely thin and parallel to each other is L , the cross-sectional area where

the current flows be A and the conductivity of the specimen in simulation be σ_s , with index “s” denoting simulation. The resistance of the specimen R_s is expressed using a correction factor δ due to effect of non-infinitesimally thin electrodes

$$R_s = \frac{1}{\sigma_s} \cdot \delta \cdot \frac{L}{A} = \frac{U_s}{I} \tag{2}$$

Meanwhile, the simulated potential difference of the inner electrodes is U_s and the applied current in simulation is I . Since δ , L and A only involve the geometry of the specimen, Eq. (2) can be written using a form factor K_s as (Ohm’s law):

$$R_s = K_s \cdot \frac{1}{\sigma_s} = \frac{U_s}{I} \tag{3}$$

$$\text{with } K_s = \delta \cdot \frac{L}{A}$$

On the other hand, the measured specimen has an unknown conductivity σ_m , with index “m” indicating measurement. So, its resistance is

$$R_m = K_m \cdot \frac{1}{\sigma_m} = \frac{U_m}{I} \tag{4}$$

The measured potential difference between the inner electrodes is U_m . Because the currents for simulation and measurement were set to have the same values, one can derive out of Eqs. (3) and (4)

$$\frac{\sigma_s U_s}{K_s} = \frac{\sigma_m U_m}{K_m} \tag{5}$$

Since the specimen in simulation has the same geometry as the specimen in the actual measurement, Eq. (6) follows

$$K_s = K_m = K \quad (6)$$

From Eqs. (5) and (6), one obtains

$$\sigma_s U_s = \sigma_m U_m = \text{const.} \quad (7)$$

$$\sigma_m = \frac{\sigma_s U_s}{U_m} = \frac{\sigma_s U_s}{I R_m} \quad (8)$$

Equations (3) and (6) lead to the form factor K_m

$$K_m = \frac{\sigma_s U_s}{I} \quad (9)$$

The described procedure to calculate the conductivity σ and the form factor K_m and its validation are summarized in Fig. 3.

For the simulation, the current I and the conductivity σ_s are input parameters for the 3D model in the FE software to simulate the potential difference of the inner electrodes U_s . I is set to have the same value as the current that will be used later in the four-wire technique. σ_s can be set as any positive value, as long as the conductivity of the electrodes in the simulation (here 10^9 S/cm) is set to be at least three magnitudes higher than σ_s . Numeric errors may occur if σ_s is too small. This problem will be addressed in the discussion part. On the other hand, the resistance of the specimen is measured by four-wire technique. Since the used current I is known, the actual potential difference is calculated by multiplying I with the measured resistance R_m , which leads to U_m . According to the above said, $\sigma_s U_s = \sigma_m U_m$. Therefore, for the unknown conductivity of the specimen $\sigma_m = \frac{\sigma_s U_s}{U_m}$ and for the form factor of the specimen

$K_m = \frac{\sigma_s U_s}{I}$ hold. To validate the calculation, the calculated σ_m is put again into the simulation with the current I to simulate a new potential difference U_{sim} . This potential difference is then compared with the measured potential difference U_m to see to which extend they agree with each other.

Method

This section explains the procedure how the geometry was obtained. It can also be considered as a kind of recipe. The following steps from taking the camera image to building up the CAD (computer-aided design) model that is imported into the FE software should be considered as an example. Therefore, only a few words are spent in the main article, but the steps are comprehensively described in Part II of the Supplementary Information.

Inside a photo light box, a scale was placed next to the specimen. The camera (here a camera of a mobile phone) was arranged above the specimens, and the camera lens was kept parallel to the surface of the specimens. The images were taken using the automatic mode. Typical images for two specimens are given in Fig. 4.

The camera images were denoised using a so-called technique “morphological anisotropic diffusion” [12, 13] followed by edge detection using a canny edge detector. The resulted edge maps were processed to vector graphics using centerline tracing technique [14]. After postprocessing such as

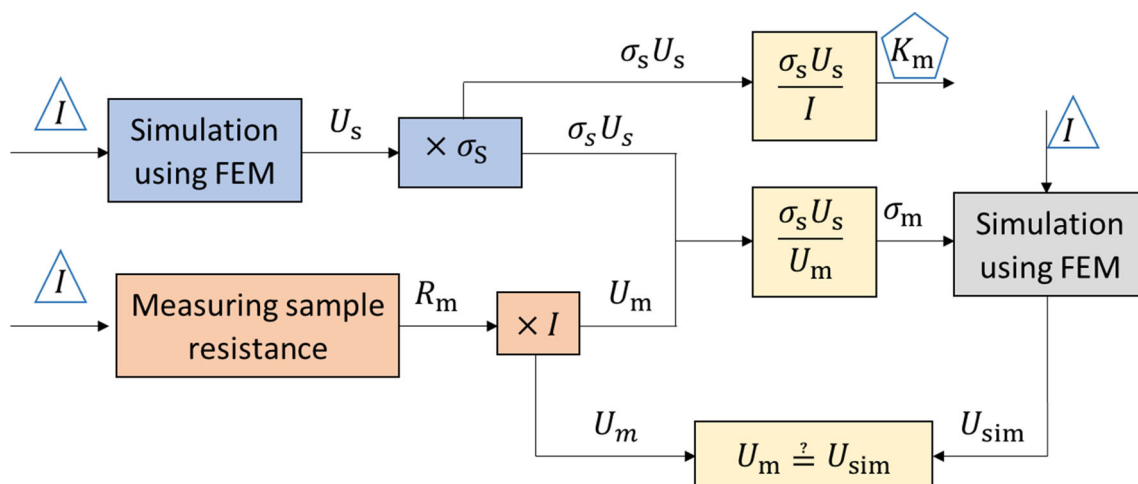
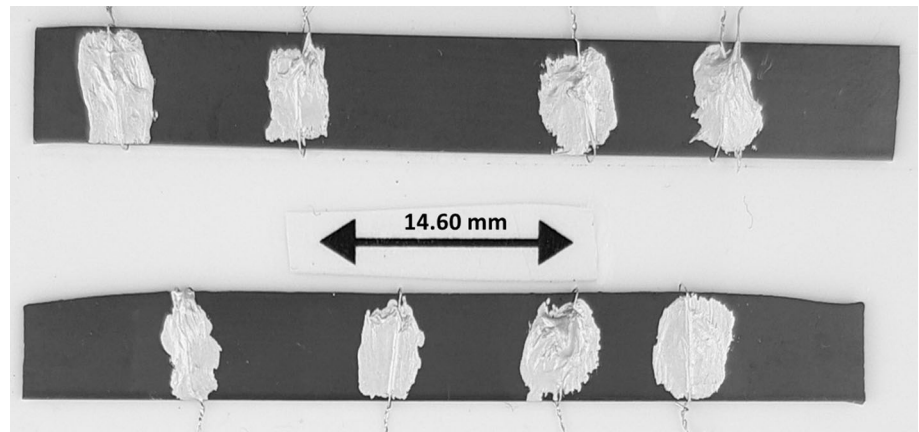


Figure 3 Procedure to calculate the conductivity, to derive the form factor K_m , and to validate it. The form factor K_m outlined with a pentagon is the output, whereas the current I outlined with a triangle is the input.

Figure 4 Image of two typical specimens A1 (top) and B1 (bottom) taken by mobile phone camera (here Samsung Galaxy S8 in automatic mode). For the meaning of the sample denotation, see text below.



eliminating artifacts, 3D extrusion in the CAD program and rescaling, the CAD models were imported into COMSOL Multiphysics. After assigning the boundary conditions, the conductivity and the form factor were calculated following the procedures illustrated in Fig. 3.

Experiments

To verify the described method above, a ceramic spinel-type NiMn_2O_4 -based block ($50 \text{ mm} \times 5 \text{ mm} \times 0.6 \text{ mm}$) provided by Vishay Electronic GmbH, Selb, Germany, was used, with a composition similar to the one described in [15]. Two specimens (sample A, sample B, with a thickness of 0.60 mm each) were cut from the block, and each specimen was contacted with four electrodes using silver wires and silver paint (Ferro, #530042). A typical specimen image is shown in Fig. 4. The resistance of each specimen was measured in a silicon oil bath where the temperature was controlled very precisely at $25 \text{ }^\circ\text{C}$ (for details of the setup see [16]). Then, the electrodes were removed and newly contacted with other electrode geometries. The experiments were conducted three times. In each experiment, the form of the electrodes was modified. The specimens are denoted as A1, A2, A3 and B1, B2, B3, respectively. They are shown in Fig. 5a. Their respective CAD plots are shown in Fig. 5b.

Results and discussion

In Table 1, the calculated form factors K_m of each specimen are shown. Between A3 and A2, the form factor differs by a ratio of 2.48. In other words, the voltage drop U_{23} would differ by a factor of almost 2.5, when applying the same current I .

Although the form factor of the specimens differs significantly within sample A and sample B, the average derived conductivity of the sample A and B is $3.613 \pm 0.249 \text{ S/cm}$ and $4.07 \pm 0.184 \text{ S/cm}$, respectively. The standard deviation of the conductivity for sample A and sample B is 6.89% and 4.52% respectively, indicating that specimens A1, A2, A3 and specimens B1, B2, B3 should be the same material. The difference in the average conductivity of sample A and sample B might be due to the fact that sample A and sample B were cut from different parts of the bulk material and inhomogeneity in the bulk material. Another explanation for the difference might be the precision of the thickness measurement. The thickness was measured by a caliper at three different positions of the specimen (near the left end, in the middle and near the right end) and an average thickness was taken as the overall thickness of the sample; however, the thickness of the specimens might not be constant and the thickness measurement has a precision of 0.05 mm; this is already approximately 8% of the total sample thickness of 0.60 mm. The measurement uncertainty of the thickness can be reduced by using a micrometer screw gauge rather than a caliper. Other errors might come from distortion of the image due to distortion caused by camera lens and denoising of the image. Nevertheless, the good agreement between measured U_{23}

Figure 5 **a** Images of the samples A1 and B1, A2 and B2, and A3 and B3 (from top to bottom) **b**: Their respective CAD plots as derived according to the described procedure. Please note that the form factors differ widely for each specimen, since the width of the electrodes was varied.

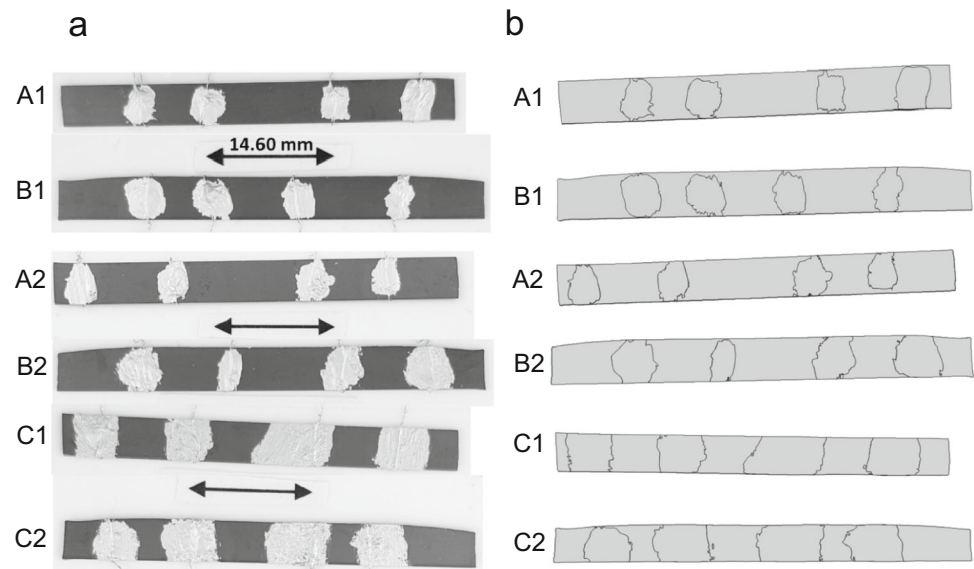


Table 1 Form factors of the specimens A1, A2, A3 and B1, B2, B3 as shown in Fig. 5, measured resistances in four-wire technique $R_m = U_{23}/I$ according to Eq. (4) and derived conductivities σ_m

Specimen	K_m/m^{-1} at 25 °C	R_m/Ω at 25 °C	$\sigma_m/10^{-4} \text{ Scm}^{-1}$ at 25 °C
A1	1882	53,704	3.505
A2	2125	56,086	3.789
A3	857	24,931	3.437
B1	1265	32,563	3.885
B2	1861	43,757	4.253
B3	1243	30,499	4.076

and U_m from the simulation using σ_m supports the validity of the proposed method.

As a side remark, one may consider the effect of temperature on the form factor. For simplicity, let us assume the thermal expansion is isotropic and the thermal expansion coefficient is α , and then, the form factor at elevated temperatures with temperature difference of $\Delta T = T - 25$ °C is:

$$K_m(T) = \delta \frac{L(1 + \alpha\Delta T)}{A(1 + \alpha\Delta T)^2} = \frac{K_m(25^\circ\text{C})}{(1 + \alpha\Delta T)} \quad (10)$$

Assuming a typical value for a thermal expansion coefficient of ceramic material of $\alpha \approx 10 \cdot 10^{-6} \text{ K}^{-1}$, and $T = 1025$ °C, i.e., $\Delta T = 1000$ °C, a deviation from the room temperature value for K_m of $\frac{1}{(1 + \alpha\Delta T)} \approx 0.99$ follows. Therefore, the form factors at 1000 °C differ only by ca. 1% from the form factors at 25 °C. In other words, the form factors obtained for a specimen at room temperature can be used for the same specimen at high temperatures. Further experiments at high temperatures are necessary to validate this theory.

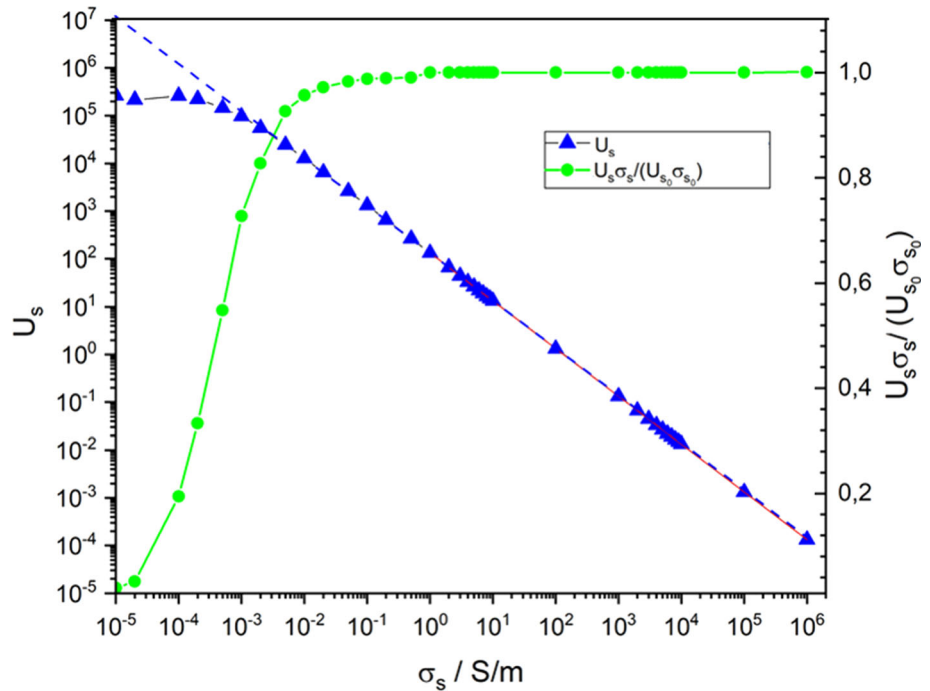
The question may arise, whether this method has limitations. Two limitations are obvious:

1. numerical errors arise if σ_s for simulation is set below 0.01 Sm^{-1}
2. the procedure is not applicable for sample with a conductivity above 10^6 Sm^{-1}

The first limitation is based on two facts derived from the simulation of the model in Fig. S1. The first fact is that the ratio $\frac{U_s \sigma_s}{U_{s0} \sigma_{s0}}$ deviates significantly from 1, when σ_s is below 0.01 Sm^{-1} (see Fig. 6). Here, U_{s0} and σ_{s0} are values from the case where the conductivity of the specimen in the simulation is 1 Sm^{-1} . Since $U_s \sigma_s = \text{const.}$ (see Eq. (7)), it is to be expected that this ratio should be 1. The second fact is that the potential difference is not on the extrapolated line, when σ_s is below 0.01 Sm^{-1} (see Fig. 6). However, the potential difference should vary linearly if potential and conductivity are plotted logarithmically (see Equations (11)–(13)).

From Eq. (7), we have:

Figure 6 Numeric errors happen for conductivities below 0.01 Sm^{-1} .



$$U_s \sigma_s = \text{const.} \tag{11}$$

Then, we have:

$$\log(U_s \sigma_s) = \log(\text{const.}) \tag{12}$$

From here, let us assume $\log(\text{const.}) = c$, as c is a constant

$$\log(U_s) + \log(\sigma_s) = c \tag{13}$$

This limitation can be circumvented by setting σ_s to be 10^5 times higher (for example, 1000 Sm^{-1}). The simulated potential difference should then be divided by 10^5 for further calculations. However, σ_s should be set at least three orders smaller than the conductivity of the electrodes in the simulation, otherwise the region of the electrode would not be an equipotential area and the assumptions for the calculation are not valid anymore. This is also the reason for the second limitation.

It should also be pointed out that in the shown example, a 2D method is used, since only the surface with the electrodes is photographed and the thickness of the specimen is assumed as constant along the length and width direction. For specimens with non-uniform thickness, the thickness profile should be taken into consideration during the extrusion of the 2D CAD sketch. Moreover, the postprocessing of the edge image into a CAD file is not yet fully automated.

Conclusion and outlook

A novel method is presented in this study that enables a precise and reliable measurement of the conductivity of a block-shaped or plate-shaped semiconductor using four-wire-technique whose electrodes have arbitrary form. It can be especially applied for high temperature conductivity measurements of ceramics. This initial work used a 2D model for planar samples. The basic idea is to reconstruct the arbitrary-shaped electrodes and the block-shaped specimen (here obtained by a camera image of the sample) into a CAD file. After that, a form factor (geometry factor) is calculated with the help of FE software. The conductivity can then be derived from the resistance measurement, preferably in four-wire technique. This method can save experimentalist time, as most of the steps in the method is automated and one does not have to spent much time ensuring that the electrodes are thin enough and/or parallel to each other in order to obtain precise results. For further development of this method, the postprocessing of the edge image into a CAD file, the import of the model and the assignment of the boundary conditions in the FE software should be fully automated. One idea for a fully automated postprocessing of the edge image is to use machine learning to detect the desirable features. An application interface can

also be written to import the CAD file into the FE software and to assign the boundary conditions automatically. Moreover, by combining this method with computer topography (CT), it can also be applied for macroporous semiconductor specimens, e.g., conductive oxides. The ultimate goal is to develop a compact application so that conductivity measurement of semiconductors can be reduced to just a four-wire measurement of the resistance and taking an image of the specimens.

Supplementary Information: The online version contains supplementary material available at (<http://doi.org/10.1007/s10853-021-05949-4>).

Acknowledgements

The authors thank Vishay Electronic GmbH, Selb, Germany, for providing the ceramic samples. The authors thank Mr. Robin Werner for supporting sample preparation.

Open Access This article is licensed under a Creative Commons Attribution 4.0 International License, which permits use, sharing, adaptation, distribution and reproduction in any medium or format, as long as you give appropriate credit to the original author(s) and the source, provide a link to the Creative Commons licence, and indicate if changes were made. The images or other third party material in this article are included in the article's Creative Commons licence, unless indicated otherwise in a credit line to the material. If material is not included in the article's Creative Commons licence and your intended use is not permitted by statutory regulation or exceeds the permitted use, you will need to obtain permission directly from the copyright holder. To view a copy of this licence, visit <http://creativecommons.org/licenses/by/4.0/>.

Funding

Open Access funding enabled and organized by Projekt DEAL.

References

- [1] Rymaszewski R (1969) Relationship between the correction factor of the four-point probe value and the selection of potential and current electrodes. *J Phys E* 2(2):170–174. <https://doi.org/10.1088/0022-3735/2/2/312>
- [2] Buehler MG, Thurber WR (1976) A planar four-probe test structure for measuring bulk resistivity. *IEEE Trans Electron Devices* 23(8):968–974. <https://doi.org/10.1109/T-ED.1976.18518>
- [3] Smits FM (1958) Measurement of sheet resistivities with the four-point probe. *Bell Syst Tech J* 37(3):711–718. <https://doi.org/10.1002/j.1538-7305.1958.tb03883.x>
- [4] Valdes LB (1954) Resistivity measurements on Germanium for transistors. *Proc IRE* 42(2):420–427. <https://doi.org/10.1109/JRPROC.1954.274680>
- [5] van der Pauw LJ (1958) A method of measuring specific resistivity and Hall effect of discs of arbitrary shapes. *Philips Res Rep* 13(1):1–9
- [6] ASTM F76–08(2016)e1: Standard test methods for measuring resistivity and hall coefficient and determining hall mobility in single-crystal semiconductors. West Conshohocken, PA. doi: <https://doi.org/10.1520/F0076-08R16E01>
- [7] Moos R, Härdtl KH (1997) Defect chemistry of donor-doped and undoped strontium titanate ceramics between 1000° and 1400°C. *J Am Ceram Soc* 80(10):2549–2562. <https://doi.org/10.1111/j.1151-2916.1997.tb03157.x>
- [8] Bishop SR, Stefanik TS, Tuller HL (2011) Electrical conductivity and defect equilibria of $\text{Pr}_{0.1}\text{Ce}_{0.9}\text{O}_{2-\delta}$. *Phys Chem Chem Phys*. 13(21):10165–10173. <https://doi.org/10.1039/c0cp02920c>
- [9] Mitoff SP (1961) Electrical conductivity and thermodynamic equilibrium in nickel oxide. *J Chem Phys* 35(3):882–889. <https://doi.org/10.1063/1.1701231>
- [10] Rothschild A, Menesklou W, Tuller HL, Ivers-Tiffée E (2006) Electronic structure, defect chemistry, and transport properties of $\text{SrTi}_{1-x}\text{Fe}_x\text{O}_{3-y}$ solid solutions. *Chem Mater* 18(16):3651–3659. <https://doi.org/10.1021/cm052803x>
- [11] Fuierer P, Maier M, Exner J, Moos R (2014) Anisotropy and thermal stability of hot-forged BICUTIVOX oxygen ion conducting ceramics. *J Eur Ceram Soc* 34(4):943–951. <https://doi.org/10.1016/j.jeurceramsoc.2013.10.016>
- [12] Segall CA, Acton ST (1997) Morphological anisotropic diffusion. *Int Conf on IP* 3:348–351. <https://doi.org/10.1109/ICIP.1997.632112>
- [13] Lopes D (2020) Anisotropic Diffusion (Perona & Malik) <https://www.mathworks.com/matlabcentral/fileexchange/14995-anisotropic-diffusion-perona-malik>), MATLAB Central File Exchange

- [14] Weigert J (2018) inkscape-centerline-trace. <https://github.com/fablbnbg/inkscape-centerline-trace>
- [15] Schubert M, Münch C, Schuurman S et al (2018) Characterization of nickel manganite NTC thermistor films prepared by aerosol deposition at room temperature. *J Eur Ceram Soc* 38(2):613–619. <https://doi.org/10.1016/j.jeurceramsoc.2017.09.005>
- [16] Schubert M, Kita J, Münch C, Moos R (2017) Analysis of the characteristics of thick-film NTC thermistor devices

manufactured by screen-printing and firing technique and by room temperature aerosol deposition method (ADM). *Funct Mater Lett* 10(06):1750073. <https://doi.org/10.1142/S1793604717500734>

Publisher's Note Springer Nature remains neutral with regard to jurisdictional claims in published maps and institutional affiliations.